Acoustic Beam Probing Using Optical Techniques

By M. G. COHEN and E. I. GORDON

(Manuscript received January 8, 1965)

In Section I it is demonstrated that the amplitude of the light deflected or scattered by an advancing sinusoidal acoustic wave, as a function of the angle between the direction of light propagation and the acoustic wavefront, is proportional to the Fourier transform of the amplitude distribution of the acoustic wave in the plane of the wavefront. Studying the angular dependence of the optical-acoustic interaction accurately and directly determines the angular distribution or far-field diffraction pattern of the acoustic beam and incidentally determines the angular response of the acoustic transducer producing the beam. The angular resolution equals the angular spread in the probing light beam. Experiments illustrating and verifying the technique are described.

In Section II the effect of volume acoustic loss is determined. It is shown that loss does not change the considerations of Section I apart from a slight reduction in angular resolution unless the decay distance is comparable to the acoustic wavelength. The loss parameter does introduce a maximum usable acoustic beam width for the interaction (coherence width). In addition, techniques for determining the acoustic loss are described. Particular attention is given to the near- and far-field energy distribution of the scattered light beam. It is shown that the far-field distribution is Lorentzian only under special circumstances. Consideration is given to probing beams with rectangular and Gaussian intensity distributions. Edge effects are taken into account, and it is shown that these can make important contributions to the line shape as well as lead to errors in the interpretation of phonon lifetimes from scattering experiments. Experiments confirming the results are described.

INTRODUCTION

It is well known that acoustic waves in transparent materials can be used to deflect or scatter light beams.[1,2] As a result, a great deal can be learned about the energy distribution in the acoustic beam by studying the angular and positional dependence of the optical-acoustic interaction.

The paper is divided into two parts. Section I is devoted to the theoretical and experimental demonstration of the fact that the amplitude of the light deflected by an advancing sinusoidal acoustic wave, as a function of the angle between the direction of light propagation and the acoustic wavefront, is proportional to the Fourier transform of the amplitude distribution of the acoustic wave in the plane of the wavefront. Thus the angular dependence of the optical-acoustic interaction accurately and directly measures the angular distribution of the acoustic energy. Stated another way, a study of the total power in the scattered light beam as a function of the angle of the light beam relative to the acoustic beam yields directly the far-field or Fraunhofer diffraction pattern of the acoustic beam.

The power in the deflected light beam measures the acoustic intensity at the position of the light beam. Absolute determination of the acoustic intensity can be made if the photoelastic constants for the medium are known. This technique is thereby capable of providing more information about the acoustic beam than can be obtained with conventional pulse-echo techniques or acoustic probes, such as described by Fitch and Dean,[3] which must be used at a boundary of the acoustic transmission medium. In particular, volume acoustic loss can be determined directly. The precise direction and phase velocity of the acoustic wave can also be determined unequivocally.

In Section 1.1, the theory of the optical-acoustic interaction in the absence of volume loss is sketched. Experiments verifying the basic concepts are described in Section 1.2.

In Section II the case of finite volume loss is considered. Particular attention is given to techniques for determining the volume loss both by probing the acoustic beam along its propagation path and by observing the far-field diffraction of the scattered light beam.

I. OPTICAL-ACOUSTIC INTERACTION IN THE ABSENCE OF VOLUME LOSS

1.1 *Theory*

The geometry of the interaction is defined in Fig. 1. The acoustic wave is propagating approximately along the x axis, and the light

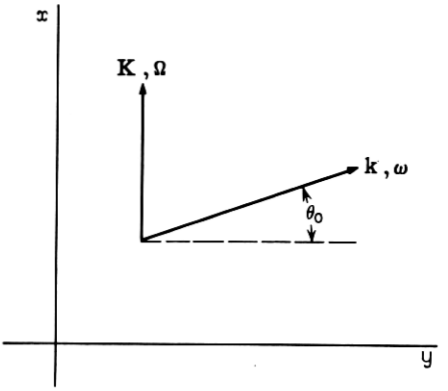

Fig. 1 — Geometry of the interaction region. The z axis is out of the plane of the paper.

beam in the x-y plane. It is assumed there is no z variation. For light with a given polarization, the photoelastic effect produces a variation in the dielectric constant which is proportional to the amplitude of the acoustic wave. The amplitude of the acoustic wave is such that the dielectric constant of the medium ϵ has a variation $\Delta\epsilon$ given by

$$\Delta\epsilon(x,y,t) = [\Delta\epsilon(y)]_c \cos(\Omega t - Kx) + [\Delta\epsilon(y)]_s \sin(\Omega t - Kx) \quad (1)$$

in which Ω is the acoustic angular frequency and K the acoustic propagation constant ($K = \Omega/v$ with v the acoustic velocity). It can be shown that the optical field E of angular frequency ω is described by the wave equation[1]

$$\partial^2 E/\partial x^2 + \partial^2 E/\partial y^2 - c'^{-2}\partial^2(1 + \Delta\epsilon/\epsilon)E/\partial t^2 = 0 \quad (2)$$

in which c' is the light velocity in the medium. In the absence of a perturbation in the dielectric constant, E is assumed to be a plane wave with propagation constant $k = \omega/c'$. As in Ref. 1, the perturbed E is expanded in a set of plane waves appropriate to the grating orders associated with a periodic index variation,

$$E(x,y,t) = \sum_{l=-\infty}^{+\infty} V_l(y) \exp i[(\omega + l\Omega)t - (k \sin\theta_0 + lK)x - ky\cos\theta_0] + \text{complex conjugate.} \quad (3)$$

The quantity $V_l(y)$ can be identified as the amplitude of the lth deflected beam of frequency $\omega + l\Omega$. The zero-order or main beam makes an angle θ_0 with the y axis in the x-y plane. The angle of deflection of the lth wave will be discussed shortly. Substituting (3) into (2) yields,

after performing the required algebra, a set of equations for the amplitudes V_l given by

$$d^2V_l/dy^2 - 2ik(\cos\theta_0)dV_l/dy + 2k(\cos\theta_0)\beta_l V_l = -\tfrac{1}{2}k^2(1 + l\Omega/\omega)[([\Delta\epsilon/\epsilon]_c + i[\Delta\epsilon/\epsilon]_s)V_{l+1} + ([\Delta\epsilon/\epsilon]_c - i[\Delta\epsilon/\epsilon]_s)V_{l-1}] \quad (4)$$

in which

$$\beta_l = [2lkK(v/c' - \sin\theta_0) - l^2K^2(1 - v^2/c'^2)]/2k\cos\theta_0 . \quad (5)$$

In the limit $\Delta\epsilon/\epsilon \ll 1$, V_l is a relatively slowly varying function of y and d^2V_l/dy^2 is negligible compared to the other terms in (4). Neglecting $\Omega/\omega \ll 1$ and defining

$$\xi(y) = \tfrac{1}{2}(k/\cos\theta_0)([\Delta\epsilon(y)/\epsilon]_c + i[\Delta\epsilon(y)/\epsilon]_s) \quad (6)$$

(4) can be rewritten (using * to denote complex conjugate)

$$dV_l/dy + i\beta_l V_l = -\tfrac{1}{2}i[\xi V_{l+1} + \xi^* V_{l-1}]. \quad (7)$$

The initial conditions are $V_l(0) = 0$ for $l > 0$, $V_0(0) = V_0$. The equation for the deflected wave amplitudes, (7), has been found by many authors for the case ξ = constant and real. Solutions have been found and are described in Ref. 1. More recent unpublished investigations[4] have yielded the same results. In what follows the major emphasis will be given to the case $\xi = \xi(y)$ and to displaying the solution in a form which has a simple physical interpretation. Consistent with the experiments to be described, it is assumed that

$$\left| \int_{-\infty}^{+\infty} \xi(y)dy \right| \ll 1$$

and it follows that $V_{l+1} \ll V_l$. Thus to a very good approximation, for $l > 0$, (7) can be integrated to yield

$$V_l(y) \approx (\exp -i\beta_l y) \int_{-\infty}^{y} dy'[-\tfrac{1}{2}i\xi(y')^* V_{l-1}(y')] \exp +i\beta_l y'. \quad (8)$$

A similar equation holds for $l < 0$ with $\xi^* V_{l-1}$ replaced by ξV_{l+1}. Inspection of (8) indicates that all the V_l will be essentially zero unless $\beta_1 L < \pi$ (in which L is a measure of the interaction length or width of the acoustic beam). An exception may hold when ξ is a rapidly varying periodic function of y. This exception is of no interest here, since it corresponds to a situation where the acoustic beam has components moving at large angles relative to the x axis. When $\beta_1 L$ is small, the rest

of the $\beta_1 L$ cannot be small unless $K^2 L/k < \pi$. When this inequality holds, many grating orders can be excited and the interaction is said to be in the Raman-Nath regime. When $K^2 L/k > \pi$ the interaction is said to be in the Bragg scattering regime and only V_1 (or V_{-1}) and V_0 can be nonzero.

In the region in which the deflected beam is observed, that is, beyond the optical-acoustic interaction region, $\xi(y) \equiv 0$ and one can without error extend the upper limit of the integration in (8) to $+\infty$. Thus the amplitude of the deflected beam can be written

$$V_1 \approx (-\tfrac{1}{2} i V_0 \exp -i\beta_1 y) \int_{-\infty}^{+\infty} dy' \xi(y')^* \exp +i\beta_1 y'. \tag{9}$$

A similar equation holds for V_{-1}. It is assumed that because

$$\left| \int_{-\infty}^{+\infty} \xi(y) dy \right| \ll 1,$$

V_0 is constant. In fact V_0 differs from its initial value by terms of order

$$\left| \int_{-\infty}^{+\infty} \xi(y) dy \right|^2$$

and higher. As an example of the error produced by this approximation, consider the case where $\xi(y)$ is constant over a length L and zero elsewhere. Equation (9) predicts

$$V_1 \sim \sin \tfrac{1}{2} \beta_1 L / \beta_1$$

while (7) predicts, in the Bragg scattering limit,[1]

$$V_1 \sim \sin \tfrac{1}{2} (\beta_1^2 + \xi^2)^{1/2} L / (\beta_1^2 + \xi^2)^{1/2}$$

which differs insignificantly when $\xi L \ll 1$. Note that V_1 becomes small when $\beta_1 L > \pi$, as noted earlier.

The quantity β_1 can be evaluated as a function of θ_0 from (5), which yields

$$\begin{aligned} \beta_{\pm 1} &= [\pm 2kK(v/c' - \sin \theta_0) - K^2(1 - v^2/c'^2)]/2k \cos \theta_0 \\ &= \pm K(\sin \Theta - \sin \theta_0)/\cos \theta_0 \end{aligned} \tag{10}$$

in which Θ is an angle defined by

$$\sin \Theta = v/c' \mp \tfrac{1}{2}(K/k)(1 - v^2/c'^2). \tag{11}$$

The upper sign corresponds to $l = +1$, while the lower sign is for $l = -1$. If v/c' were zero, Θ would exactly equal the Bragg angle for scattering off the acoustic wavefront. In actuality the scattering plane

is rotated from the acoustic wavefront by an angle very closely equal to v/c', which for acoustic waves can be neglected. In recognition of this fact Θ will be referred to as the Bragg angle.

Substituting (10) into (9) yields

$$V_1(\theta_0) \approx (-\tfrac{1}{2}iV_0 \exp +iKy(\sin\theta_0 - \sin\Theta)/\cos\theta_0) \times \int_{-\infty}^{+\infty} dy'\xi(y')^* \exp -iKy'(\sin\theta_0 - \sin\Theta)/\cos\theta_0 . \quad (12)$$

As stated earlier, the amplitude of the deflected wave, resulting from an interaction at angle θ_0, is proportional to the Fourier transform of the acoustic wave amplitude. The relative intensity of the deflected light beam is given by $|V_1/V_0|^2$. Since $\xi(y)$ varies as $(\cos\theta_0)^{-1}$ [see (6)], the substitution $y'' = y'/\cos\theta_0$ puts (12) into a form which can be recognized as the expression for far-field or Fraunhofer diffraction for waves with propagation constant K. Thus $|V_1(\theta_0)|^2$ determines the far-field diffraction pattern of the acoustic beam.

The integral in (12) may also be interpreted by noting that an acoustic plane wave moving at a small angle ψ with respect to the x axis in the x-y plane can be described by a variation

$$\cos[\Omega t - Kx\cos\psi + Ky\sin\psi] = \cos[Ky\sin\psi] \cdot \cos[\Omega t - Kx\cos\psi] - \sin[Ky\sin\psi]\sin[\Omega t - Kx\cos\psi].$$

From (1) and (6) it follows that

$$\xi(y) = \text{constant} \times \exp -iKy\sin\psi. \quad (13)$$

Inserting this value of ξ into the integral in (12) indicates that the deflected intensity is nonvanishing only for

$$\tan\psi = (\sin\theta_0 - \sin\Theta)/\cos\theta_0$$

or, since ψ is small, for $\psi \approx \theta_0 - \Theta$. Hence the deflected light intensity, when the main beam moves at angle θ_0, measures only the component of the acoustic beam moving at angle $\psi \approx \theta_0 - \Theta$ relative to the x axis. By studying the variation of the deflected light intensity as a function of the angle θ_0 one determines the angular distribution of the acoustic energy. Since the diffraction angle of the light can, in practice, be kept small ($<10^{-4}$ radians) the angular resolution can be quite adequate except for the case of very high-frequency ($>10^{10}$ cps) acoustic waves.

From the above discussion it follows that for acoustic beams of finite width θ_0 will never differ much from Θ and (12) can be written

$$V_1(\theta_0) \approx [-\tfrac{1}{2}iV_0 \exp +iK(\theta_0 - \Theta)y] \times \int_{-\infty}^{+\infty} dy'\xi(y')^* \exp -iK(\theta_0 - \Theta)y'. \tag{14}$$

The equation for V_{-1} is the negative complex conjugate of (14) with the appropriate value of Θ for $l = -1$.

The angle of the deflected beam can be determined directly from (3). The lth deflected beam appears at an angle θ_l relative to the y-axis in the x-y plane defined by

$$(1 + \Omega/\omega) \sin \theta_l = \sin \theta_0 + lK/k. \tag{15}$$

In what follows $\Omega/\omega \ll 1$ will be neglected and only the case $l = \pm 1$ will be considered. Thus (15) can be rewritten [using (11)] as

$$\sin \theta_l = \sin \theta_0 - 2 \sin \Theta. \tag{16}$$

Defining the deflected angle as $\theta_l - \theta_0$, (16) can be solved to yield

$$\theta_l - \theta_0 \approx -2\Theta - (\Theta - \theta_0)^2 \tan \theta_0 . \tag{17}$$

Terms of order $(\Theta - \theta_0)^4$ and higher have been neglected. The deflection angle has a magnitude very closely equal to $2 \mid \Theta \mid$ and the variation in $\theta_l - \theta_0$ is quite small when θ_0 is varied through a small angle about Θ. This fact will prove to afford considerable experimental convenience.

When discussing the experimental results two distributions of acoustic intensity will be of interest. The angular dependence of the deflected intensity will be reviewed here to provide continuity in the discussion of the experiments.

Case I: A single acoustic beam of rectangular cross-section (see Fig. 2a).

For this case the acoustic beam of width L is assumed to have a constant amplitude

$$\xi(y) = \xi \qquad -\tfrac{1}{2}L \leqq y \leqq \tfrac{1}{2}L$$
$$= 0 \qquad \text{elsewhere}$$

and

$$V_1(\theta_0) = (-\tfrac{1}{2}i\xi^* V_0 \exp +iK(\theta_0 - \Theta)y)$$

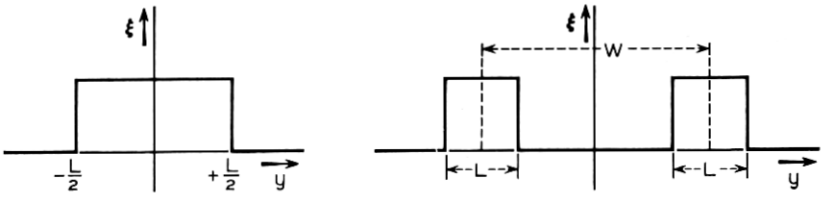

Fig. 2 — Schematic representation of acoustic beam cross-sections; (a) single beam, (b) parallel coherent beams.

$$\cdot \int_{-\frac{1}{2}L}^{+\frac{1}{2}L} dy' \exp -iK(\theta_0 - \Theta)y' \tag{18}$$

$$= (-\tfrac{1}{2}i\xi^* L V_0 \exp +iK(\theta_0 - \Theta)y) \left[\frac{\sin \frac{1}{2}K(\theta_0 - \Theta)L}{\frac{1}{2}K(\theta_0 - \Theta)L}\right].$$

The angular dependence is precisely the same as that for single-slit Fraunhofer diffraction. Note that the first zeros on either side of the central maximum are separated by an angle

$$\Delta\theta_0 = 4\pi/KL \tag{19}$$

which is a direct measure of the acoustic beamwidth L.

Case II: Two parallel coherent acoustic beams with phase difference ϑ (see Fig. 2b).

From (6) it follows that

$$\xi(y) \cos(\Omega t - Kx - \varphi) \rightarrow \xi(y)(\exp i\varphi) \cos(\Omega t - Kx)\dagger$$

hence

$$\begin{aligned} \xi(y) &= \xi && -\tfrac{1}{2}(W + L) \leqq y \leqq -\tfrac{1}{2}(W - L) \\ &= \xi \exp i\varphi && \tfrac{1}{2}(W - L) \leqq y \leqq \tfrac{1}{2}(W + L) \\ &= 0 && \text{elsewhere.} \end{aligned}$$

Each beam has width L and the center-to-center spacing is W. For this case

$$V_1(\theta_0) = (-\tfrac{1}{2}i\xi^* V_0 \exp iK(\theta_0 - \Theta)y) \cdot \left[\int_{-\frac{1}{2}(W+L)}^{-\frac{1}{2}(W-L)} dy' \exp -iK(\theta_0 - \Theta)y'\right.$$

† This is not an equality but is written to indicate that a change in the phase of the acoustic wave implies an equivalent change in the argument of $\xi(y)$.

$$+ (\exp -i\varphi) \int_{\frac{1}{2}(W-L)}^{\frac{1}{2}(W+L)} dy' \exp -iK(\theta_0 - \Theta)y' \Big] \qquad (20)$$

$$= (-i\xi^* L V_0 \exp i[K(\theta_0 - \Theta)y - \tfrac{1}{2}\varphi]) \left[\frac{\sin \frac{1}{2}K(\theta_0 - \Theta)L}{\frac{1}{2}K(\theta_0 - \Theta)L}\right.$$

$$\times \cos \tfrac{1}{2}[K(\theta_0 - \Theta)W + \varphi]\Big].$$

As would be expected, the angular dependence is precisely the same as for double-slit Fraunhofer diffraction (Young's experiment).

One other point is perhaps worth noting in passing. The relative intensity of the deflected light beam at the optimum angle is given by

$$|\tfrac{1}{2}\xi L|^2 = \tfrac{1}{16}[(\Delta\epsilon/\epsilon)_c^2 + (\Delta\epsilon/\epsilon)_s^2]k^2L^2/\cos^2\theta_0$$

which is directly proportional to the acoustic power. Quantitative determination of the acoustic power in the transmission medium can be made if the photoelastic and elastic constants of the material are known. Thus direct measurements of transducer efficiency can be made.

1.2 *Experiment*

The experiments to be described were performed using ultrasonic waves in the frequency range 50–250 mc/s. The transmission medium was fused quartz ($v = 5.96 \times 10^5$ cm/s) with rectangular cross-section of $\frac{1}{4} \times \frac{1}{2}$ inch and length one inch. A thin-film cadmium sulphide longitudinal wave transducer was evaporated onto one end of the delay line.† The faces through which the light entered and left the medium were optically flat and parallel and were antireflection coated for 6328-Å radiation. In some cases the face opposite the transducer was terminated with a mercury pool, which reduced the reflected amplitude by about 10 db.

Light from a 6328-Å He-Ne laser operating in the lowest-order transverse mode with a power of a few milliwatts was polarized at 45° to the direction of acoustic propagation. The acoustically produced strain makes the quartz uniaxial; for longitudinal acoustic waves the optic axis is along the direction of propagation. Hence, for the geometry employed, the privileged axes corresponded closely to the x and z axes and $\Delta\epsilon$ for E_z differed from $\Delta\epsilon$ for E_x. As a result the deflected beam polarization was rotated from the 45° position. This was convenient experimentally, since the zero-order or main beam could be effectively eliminated with a crossed analyser without drastically attenuating the

† The transducers were prepared by N. F. Foster.

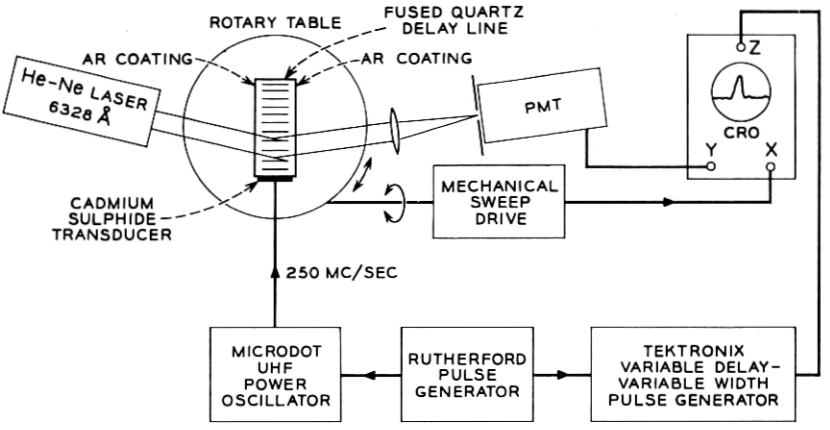

Fig. 3 — Experimental arrangement for observing angular dependence of deflected light intensity.

deflected beam. A lens focused the deflected beam through a narrow slit mounted in front of a photomultiplier. Deflection angles were of the order of one degree.

The experimental arrangement is shown in Fig. 3. When necessary the acoustic energy was pulse modulated. A mechanical table rotator was also used since, as noted earlier, the angular position of the deflected beam was essentially independent of the orientation of the acoustic wave relative to the incident light beam, and it was unnecessary to change the photomultiplier or laser position as θ_0 was varied. Thus by supplying a voltage proportional to the angular rotation of the table to the X axis of the oscilloscope and the photomultiplier output to the Y axis, the deflected energy as a function of θ_0 could be displayed. A baseline was produced by pulse modulation of the acoustic energy.

A typical display is shown in Fig. 4 and very closely follows the predicted $[\sin \frac{1}{2}K(\theta_0 - \Theta)L/\frac{1}{2}K(\theta_0 - \Theta)L]^2$ behavior for a single acoustic beam of rectangular cross-section. It should be noted that the angle θ_0 is that of the light within the medium and is smaller by the factor $n = 1.46$ than the angle measured on the table because of refraction in the quartz. (Severe errors are introduced when the surfaces are not optically antireflection coated, because of multiple reflection. The multiple reflection can be used to greatly enhance the optical-acoustic interaction and will be discussed in more detail in a forthcoming paper.) Using (19), the measured acoustic beamwidth corresponded very closely to the width of the transducer. For very wide transducers (>2 cm)

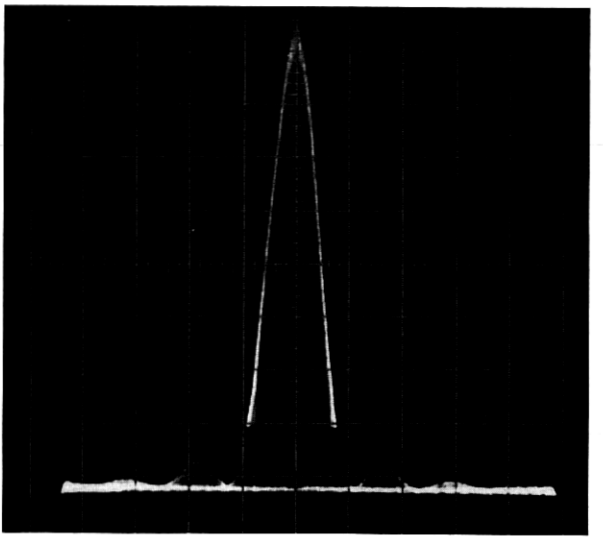

Fig. 4 — The angular dependence for a rectangular beam cross-section which closely followed the theoretical $(\sin x/x)^2$ behavior. The angular separation between zeros adjacent to the central peak was 0.6° at the frequency of 248 mc; using this value in (19) one calculates the width of the acoustic beam to be 4.2 mm, which corresponds very closely to the width of the transducer. The peak deflected light intensity was in the range 0.1 to 1 per cent of the intensity of the zero-order beam. The acoustic intensity was of the order of 0.1 watt/cm^2.

deviations from the ideal $(\sin x/x)^2$ behavior were observed and ascribed to nonuniform transducers and finite resolution associated with diffraction of the light. The width of the beam was still described by (19), however.

The angle for optimum interaction, $\theta_0 = \Theta$, is predicted by (11). The difference between Θ for deflection into the $l = +1$ beam (Θ_+) and Θ for deflection into the $l = -1$ beam (Θ_-) is given by

$$\begin{aligned} \Theta_+ - \Theta_- &\approx \sin \Theta_+ - \sin \Theta_- \\ &= -K/k = -(\Omega/\omega)(c'/v) \end{aligned} \tag{21}$$

using (11) with $v^2/c'^2 \ll 1$. Direct verification of (21) in the range $\Omega/2\pi = 50$–250 mc/s was obtained by using a narrow slit in front of the photomultiplier and determining the angular difference between the peaks of the $(\sin x/x)^2$ curves for $l = \pm 1$.

The angle of deflection is given as $\theta_l - \theta_0 \approx (lK/k)$. This was verified also for $l = \pm 1$. No higher orders were observed, consistent with the

fact that $K^2L/k > \pi$, placing the interaction in the Bragg scattering regime.

It is interesting to note that when the delay line is unterminated an acoustic standing wave is established. The $l = +1$ deflected wave at frequency $\omega + \Omega$ associated with one of the traveling acoustic waves, and the $l = -1$ wave at frequency $\omega - \Omega$ associated with the oppositely moving acoustic wave are deflected into the same angle [see (16)] and can mix in the photodetector. A beat at the difference frequency $2(\Omega/2\pi)$ was detected, and it was found as expected that the light was essentially 100 per cent modulated. The amplitude of the beat as a function of θ_0 also followed the $(\sin x/x)^2$ variation.

Fig. 5 illustrates the results of an experiment in which the frequency of the acoustic wave was swept periodically. When the deflected beam was allowed to travel several feet and fall on the wall of the room the reciprocating motion of the beam could easily be observed. The oscilloscope display shows the output of the photomultiplier as a function of the acoustic frequency. The horizontal axis is approximately linear with acoustic frequency. The narrow slit in front of the photomultiplier sampled the Gaussian light distribution in the deflected beam as it was swept across the slit. The "frequency width" of the beam using (16) agreed well with the "angular width" of the beam associated with diffraction. Successive photographs (top to bottom) show decreasing sweep rates and sweep widths. When the sweep rate was sufficiently slow, the acoustic resonances, separated by approximately 120 kc/s, built up the acoustic energy to its steady-state value as seen in the bottom photograph. The unequal spacing of the acoustic resonances can be attributed to some residual FM in the swept oscillator which produced a slightly nonuniform frequency base. The vertical gain was kept constant, and it can be seen that no great advantage was obtained in the resonant condition because the acoustic Q was not very high. The attenuation of the fused quartz was measured to be 0.6 db/cm or about 4.5 db for the round trip.

An interesting property of the transducer was uncovered during the course of the experiments. The far end of the delay line was unterminated and the driving signal was pulse modulated with pulses short compared to the length of the delay line but long compared to the width of the optical beam. The spacing between applied pulses was sufficiently long that there was no overlap between each successive decaying pulse train. Synchronized, variable-delay pulses were applied to the Z axis of the oscilloscope with the correct timing so that the optical-acoustic interaction was observed for only one of the pulses in the

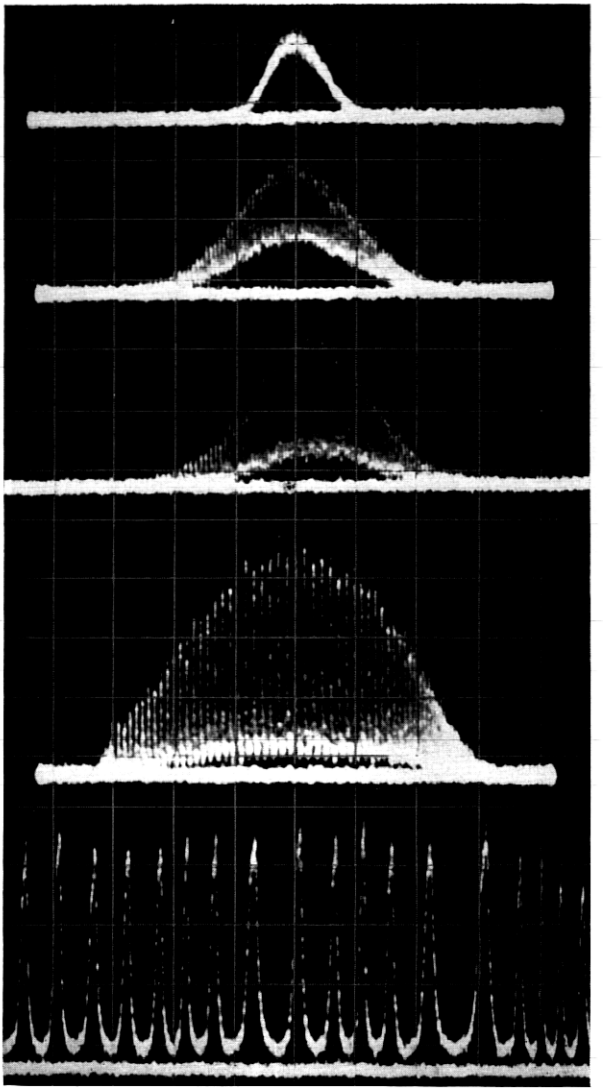

Fig. 5 — Light intensity at a fixed angular position as a function of acoustic frequency. The photomultiplier samples the intensity of the approximately Gaussian beam as it is swept across the defining slit.

decaying train. Successive pulses in the train could be studied by increasing the delay.

Fig. 6 illustrates the appearance of the $(\sin x/x)^2$ display associated with each of the pulses in the train. Multiple exposures were taken to

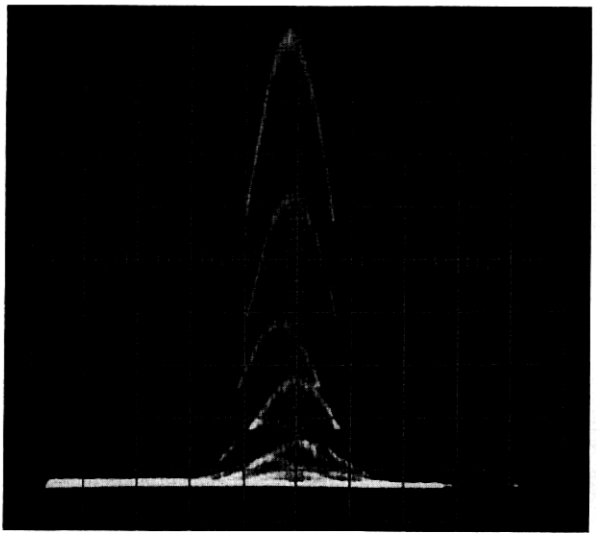

Fig. 6 — Multibounce appearance of optical-acoustic interaction indicating angular divergence of successively reflected beams. The angular divergence is less than 0.1°.

record the data on one photograph. In addition, each exposure covered about 20–50 angular sweeps and each angular sweep covered many thousands of pulses. Thus there is no doubt that the data were entirely reproducible and that the observed displacement of the optimum angle for successive pulses in the train was real.

The photograph can be interpreted in the following way. The face of the delay line opposite the transducer was optically flat and parallel to the transducer face. Thus, if the acoustic wave were launched in a direction normal to the face, it would be expected to follow the same path after reflection from the opposite face at normal incidence (see Fig. 7). For the first passage of the forward pulse, the peak of the $(\sin x/x)^2$ curve indicates the optimum angle for the $l = 1$ interaction and, incidentally, marks the precise direction of the first forward wave. If the first backward pulse were exactly parallel to the first forward pulse, the peak of the $l = -1$ interaction should have appeared at precisely the same angle, although reduced in amplitude because of the acoustic loss. This is seen to be the case. However, the second forward pulse was slightly displaced in angle from the first forward pulse, indicating that it was not parallel to the first forward pulse. Since the opposite face should reflect specularly, the second backward pulse

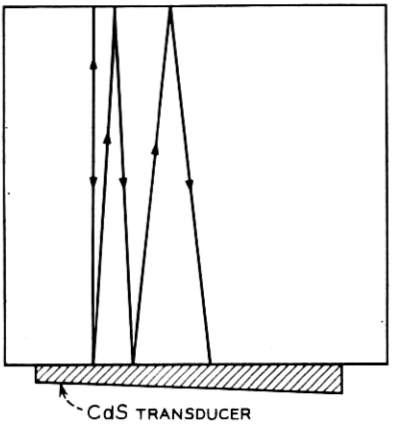

Fig. 7 — Postulated paths of successively reflected beams. The angular spread is greatly exaggerated.

should have been displaced by the same angle from the first backward pulse except in the opposite direction. This is also seen to be the case. The third forward pulse was displaced again from the second forward pulse by the same amount and in the same direction as the second was displaced from the first.

The behavior of these and succeeding pulses (see Fig. 7) can be explained by assuming that reflection of the transducer face was specular with respect to a surface which was not parallel to the opposite face. This could happen if the transducer were wedge-shaped but somehow launched an acoustic wave normal to the delay line interface. Such behavior could introduce spurious results in conventional pulse-echo experiments, since the angular dependence of the transducer response is given essentially by the same $(\sin x/x)^2$.

Further corroboration of the angular variation appeared when the delay line was allowed to resonate. The acoustic intensity in the beam cross-section showed variations which did not appear in the pulsed beam.

A more critical test of the Fourier transform relation between the acoustic intensity and the angular dependence of the deflected beam was performed using the arrangement shown in Fig. 8. In this case two identical terminated delay lines were separated by a fused quartz parallel flat. The 250 mc/s signal was divided, isolated, and applied to each transducer with a variable phase difference. The characteristic $(\sin x/x)^2$ behavior for each delay line individually peaked at the same

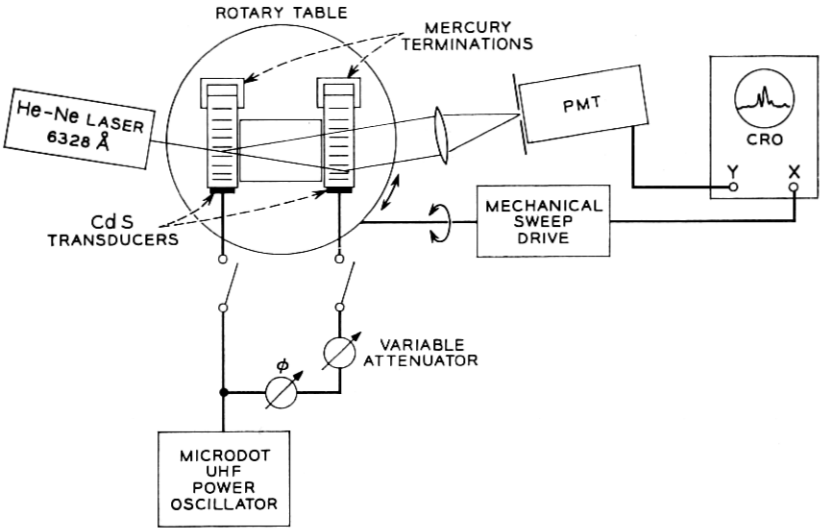

Fig. 8 — Experimental arrangement for double acoustic beam interaction.

angle and with the same amplitude, indicating that the acoustic beams were aligned and had the same intensity.

The photograph in Fig. 9 exhibits the behavior predicted by (20). The envelope has the behavior $[\sin \frac{1}{2}K(\theta_0 - \Theta)L/\frac{1}{2}K(\theta_0 - \Theta)L]^2$ superimposed on the $\cos^2 \frac{1}{2}[K(\theta_0 - \Theta)W + \varphi]$ behavior required by the spacing W. The lack of a perfect zero can be ascribed to the finite angular spread of the light beam, which was not negligibly small compared to the spacing between minima, $2\pi/KW$, and thereby tended to slightly wash out the perfect $\cos^2 x$ behavior. The observed number and spacing of the minima are consistent with the spacing W. In Fig. 10 the upper photograph was taken for $\varphi = 0$ and the lower photograph for $\varphi = \pi/2$. The peak deflected intensity is four times that for each beam, in agreement with (20).

II. FINITE VOLUME LOSS

2.1 *Theory*

When the acoustic beam is attenuated, (1), which describes the acoustic wave propagation, must be modified by including a factor $\exp -\alpha x$, in which 2α is the reciprocal decay distance for the acoustic energy. If the intensity of the acoustic wave is sufficiently low that the conditions of Section I

$$(|\int \xi \, dy| \ll 1)$$

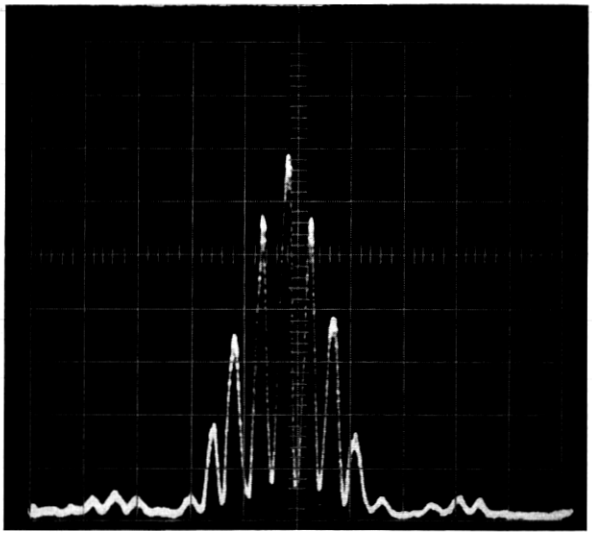

Fig. 9 — The angular distribution for two coherent acoustic beams.

are satisfied, then a suitable solution for the deflected light amplitude can be written

$$E(x,y,t) = \sum_{l=-\infty}^{+\infty} V_l(y) \exp -|\, l \,|\alpha x \exp i[(\omega + l\Omega)t - (k \sin \theta_0 + lK)x - ky \cos \theta_0] + \text{complex conjugate.} \tag{22}$$

Note that (22) differs from (3), the solution for the nondecaying acoustic beam, by the factor $\exp -|\, l \,|\alpha x$ associated with the lth deflected beam. Substituting into (2) yields an equation identical to (4) except that the term in V_{l+1} (for $l > 0$) has the factor $\exp -2\alpha x$. Therefore, strictly speaking, (22) is not a proper solution. However, when $V_{l+1} \ll V_{l-1}$, to a very good approximation, (22) represents the scattered wave amplitudes and V_l is defined by (4). One additional difference arises: the term β_l is no longer given by (5) but rather must be written

$$\beta_l' = \beta_l + il\alpha(\sin \theta_0 + lK/k)/\cos \theta_0 \tag{23}$$

in which β_l is given by (5). A term in $(\alpha/K)^2 \ll 1$ has been left out. The significant point here is that β_l' can never be zero even when $\theta_0 = \Theta$, corresponding to the optimum deflection condition. In this

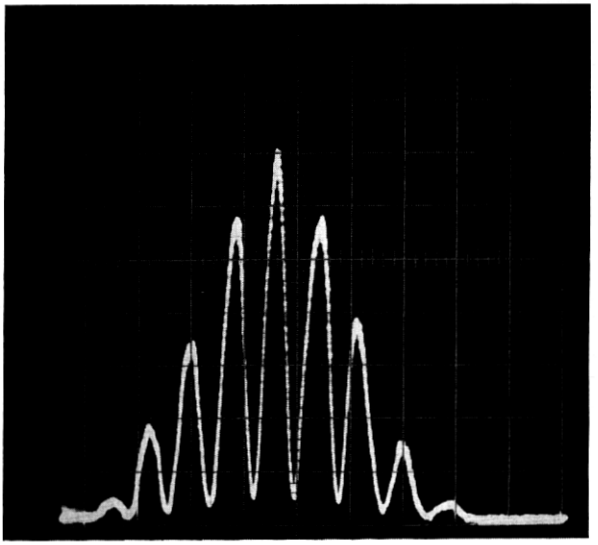

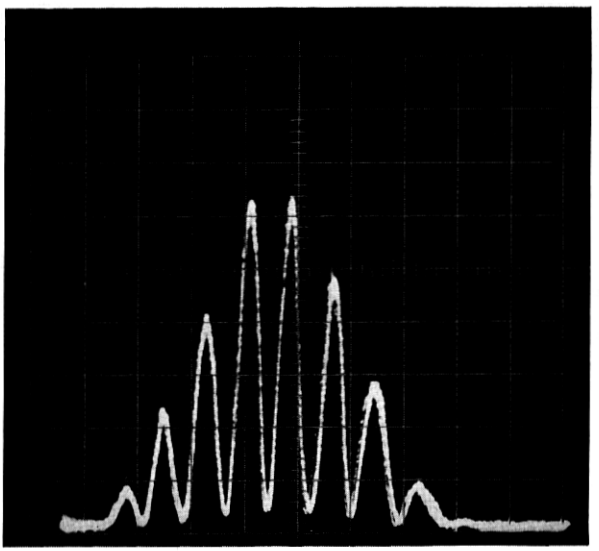

Fig. 10 — The angular distribution for $\varphi = 0$ (upper) and $\varphi = \pi/2$ (lower).

region, which is the only region of interest, $K/k \approx -2 \sin \theta_0$ and β_1' can be written

$$\beta_1' \approx \beta_1 - i\alpha \tan \theta_0 . \tag{24}$$

With the substitution of β_1' for β_1 all the results of Section I are valid for the angular dependence of the optical-acoustic interaction. Thus

$$-K(\theta_0 - \Theta) \rightarrow -K(\theta_0 - \Theta) - i\alpha \tan \theta_0 . \tag{25}$$

As an example of the consequences of this substitution, consider the angular dependence of the scattered intensity $|E_1(\theta_0, x)|^2$ corresponding to $l = 1$. For finite α, (18), derived for a rectangular distribution and an infinitely wide light beam, becomes

$$|E_1(\theta_0, x)|^2 = [\exp -2\alpha x - \alpha L \tan \theta_0] \cdot \frac{|\sin \tfrac{1}{2}[K(\theta_0 - \Theta) + i\alpha \tan \theta_0]L|^2}{\tfrac{1}{4}[K^2(\theta_0 - \Theta)^2 + \alpha^2 \tan^2 \theta_0]L^2} . \tag{26}$$

Nonessential constants have been suppressed and $|E_1|^2$ normalized so that it has the value unity for $\theta_0 = \Theta$, $\alpha = 0$. This result has a straightforward interpretation. Since the scattered beam has an exponential decay in the cross section, the effective beamwidth is of order $(2\alpha)^{-1} \cos \theta_0$ and the angular spread is $2\alpha/k \cos \theta_0$.† The product $K(2\alpha/k \cos \theta_0)$ gives rise to the term $\alpha \tan \theta_0$ in (26) and limits the angular resolution in observing the variation of $|V_1(\theta_0)|^2$.

For scattering at the Bragg angle, $\theta_0 = \Theta$,

$$|E_1(\Theta, x)|^2 = \frac{[\exp -2\alpha x - \alpha L \tan \Theta] \sinh^2 \tfrac{1}{2}\alpha L \tan \Theta}{\tfrac{1}{4}\alpha^2 L^2 \tan^2 \Theta} . \tag{27}$$

It is instructive to note that this result can be obtained from a very simple ray picture of the scattering interaction. Consider Fig. 11, which shows a typical scattered ray for interaction at the Bragg angle. Along this path, defined by $x = x_0 + y \tan \Theta$, the contributions from each scattering point are additive and proportional to the product of the acoustic and light amplitude. Thus one can write for the normalized scattered intensity

$$|E_1(\Theta, x_0)|^2 = \left| L^{-1} \int_0^L dy \exp -\alpha(x_0 + y \tan \Theta) \right|^2 . \tag{28}$$

Evaluating the integral yields a result identical to that given by (27).

† See (36).

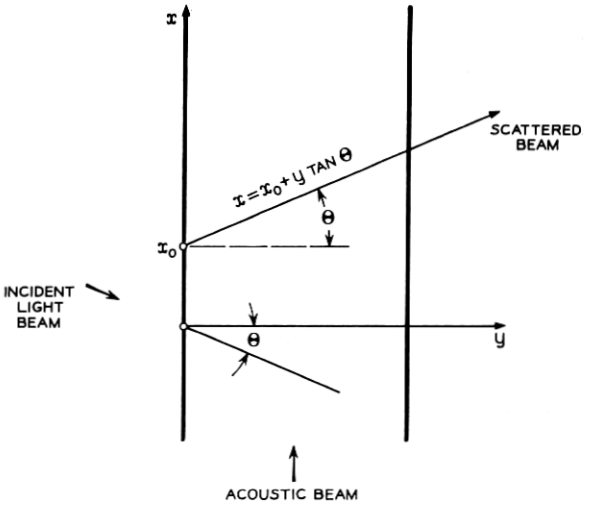

Fig. 11 — A typical scattered ray for interaction at the Bragg angle.

Note that the intensity of the scattered light is reduced from its value at $\alpha L = 0$ and can be related directly to the decreasing amplitude of the acoustic wave along the ray path. This effect will be referred to as "finite coherence width," which arises because of the acoustic decay and defines a maximum useful acoustic beam width $L = (\alpha \tan \Theta)^{-1}$. Note that the coherence width is important relative to the considerations of Section I only for $\alpha \approx K$.

In what follows the relatively simple geometrical picture described above will be exploited to determine the near-field distribution of the scattered light from incident light beams with a Gaussian intensity distribution as well as for uniform beams of finite width. From this it will be possible to calculate the shape of the far-field diffraction pattern of the scattered light. Experimental confirmation of these far-field distribution patterns, which will be described later, constitutes a much more rigorous test of the theory than direct observation of the near-field pattern. In addition, it often offers considerable experimental convenience.

2.2 *Diffraction of the Scattered Light*

The results of the previous section indicate that when the acoustic wave amplitude decays as exp $-\alpha x$ then the scattered beam will have superposed on its normal spatial dependence the factor exp $-\alpha x$. Thus,

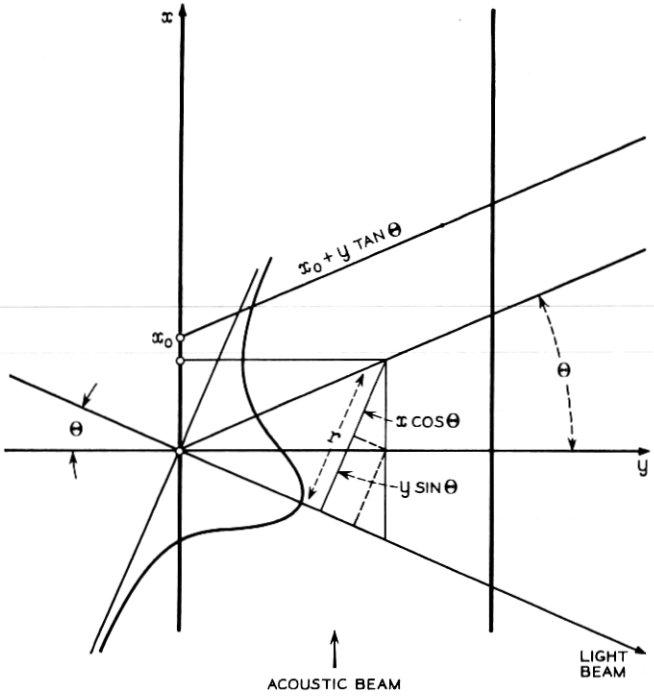

Fig. 12 — Beam with Gaussian amplitude distribution incident at the Bragg angle.

if the light beam is translated in the x direction by an amount Δx, the scattered light energy will be changed by an amount $\exp -2\alpha\Delta x$ independent of the width of the light beam. Thus it is not necessary to use narrow light beams to probe the exponential decay of the acoustic energy.

In cases where it is inconvenient or undesirable to translate the light beam relative to the acoustic beam, the decay constant can be determined by studying the near-field decay of the scattered light beam in a direction parallel to the acoustic beam. In performing this experiment, it is convenient to use a Gaussian beam as obtained directly from a gas laser (TEM_{00} mode). However, the beam must be modified, as can be seen from the following discussion.

If the incident beam has a Gaussian distribution, so that

$$E_0(x,y) = \exp -\tfrac{1}{2}\left[\frac{x \cos \Theta + y \sin \Theta}{w}\right]^2 \qquad (29)$$

as shown in Fig. 12, in which w is related to the spot size of the beam,

then it is shown in Appendix A that the scattered beam amplitude can be written

$$E_1(\Theta,x_0) = \exp -(\alpha x_0 + \tfrac{1}{2}(x_0/w)^2 \cos^2 \Theta) \times \left\{ X^{-1} \exp Y^2 \left[\int_0^{Y+X} \exp -y^2 dy - \int_0^{Y} \exp -y^2 dy \right] \right\} \tag{30}$$

with

$$X = \sqrt{2}\ (L/w) \sin \Theta$$
$$Y = \tfrac{1}{4}\sqrt{2}\ (\alpha w/\cos \Theta + 2(x_0/w) \cos \Theta)$$

where the variable x_0 denotes that the scattering originates from a point $x = x_0$, $y = 0$ on the incident beam. When $X \ll 1$, the term in braces can be expressed as

$$1 - \tfrac{1}{2}[\alpha L \tan \Theta + (x_0/w)(L/w) \sin 2\Theta]. \tag{31}$$

The term $\alpha L \tan \Theta$ arises from the coherence width of the acoustic beam. In fact, for $w \to \infty$, (30) and (27) are identical. The linear term x_0 indicates that the distribution is no longer perfectly Gaussian nor is it symmetrical. Except for this slight deviation, however, the distribution is a displaced Gaussian with the same spot size as the incident beam. Thus the scattered beam shape contains essentially no information concerning the decay constant of the acoustic wave. This situation can be changed merely by partly blocking the incident Gaussian beam so that, for example, the part of the beam described by x less than some value x_0 is removed. Under this circumstance the shift in the peak of the Gaussian can be discerned and α can be determined. Alternately, the far-field diffraction of the scattered light beam can be observed. This is given by

$$V_1(\theta) = \int_{x_0}^{+\infty} dx E_1(\Theta,x) \exp -ik(\sin \theta - \sin \Theta)x. \tag{32}$$

Using $E_1(\Theta,x)$ as given in (30), neglecting the small change resulting from the term in braces, yields

$$V_1(\eta) = \sqrt{\pi/2}\ w^{-1} \cos \Theta\ [\exp \tfrac{1}{2}\alpha^2 w^2 (1 + i\eta)^2/\cos^2 \Theta] \cdot \operatorname{erfc}\ [(x_0/\sqrt{2}\ w) \cos \Theta + \alpha w(1 + i\eta)/\sqrt{2} \cos \Theta] \tag{33}$$

in which erfc denotes the complementary error function and

$$\eta = (k/\alpha)(\sin\theta - \sin\Theta). \tag{34}$$

For the unblocked beam ($x_0 = -\infty$), the scattered intensity has the form, exclusive of constants,

$$|V_1(\eta)|^2 \propto \exp \alpha^2 w^2 \eta^2/\cos^2\Theta = \exp k^2 w^2 (\sin\theta - \sin\Theta)^2/\cos^2\Theta$$

which, as would be expected, is Gaussian in angular distribution. In particular, the angular spread is independent of α. Contrast this behavior with the situation in which approximately half the Gaussian beam is blocked, so that $|x_0/w| \ll 1$ and the beam is wide compared to the acoustic decay distance $\alpha w \gg 1$. In this limit
(using $\operatorname{erfc} z \underset{\lim z\to\infty}{=} (\sqrt{\pi}\, z)^{-1} \exp -z^2$)

$$|V_1(\eta)|^2 \propto 1/(1 + \eta^2) \tag{35}$$

which is Lorentzian with an angular width at half power determined by (using 34)

$$\Delta\theta \approx 2\alpha/k \cos\Theta. \tag{36}$$

It is perhaps instructive to rewrite the parameter η in a slightly different form. Suppose an experiment is performed, similar to that associated with Fig. 5, in which the scattered light beam is observed at a fixed angle Θ but the acoustic frequency is varied. Clearly the angle θ can be considered to represent the peak of the energy distribution as a function of the acoustic frequency. Using (15), which defines the scattering angle for a given acoustic frequency and a given $\mathbf{k}$, η can be written

$$\eta = 2(\Omega - \Omega_0)\tau \equiv 2(\omega - \omega_0)\tau \tag{37}$$

in which Ω_0 is the acoustic frequency corresponding to interaction at angle Θ and Ω corresponds to angle θ. The parameter $\tau = (2\alpha v)^{-1}$ corresponds to the phonon lifetime if $(2\alpha)^{-1}$ is interpreted as the phonon mean-free path. As would be expected, the full width of the Lorentzian at half power is τ^{-1}. The difference $\Omega - \Omega_0$ also appears at the optical frequencies.

The basic conclusion here is that one can study phonon lifetimes (or mean-free paths or acoustic decay distances) by observation of the Lorentzian linewidth in a scattering experiment such as described, but one cannot use a full Gaussian beam such as might be obtained from a gas laser. Rather, a half-Gaussian beam whose width is large compared to the decay distance is required. A discussion of this result relative to the case of Brillioun scattering with thermally generated phonons is beyond the scope of this paper and is reserved for future consideration.

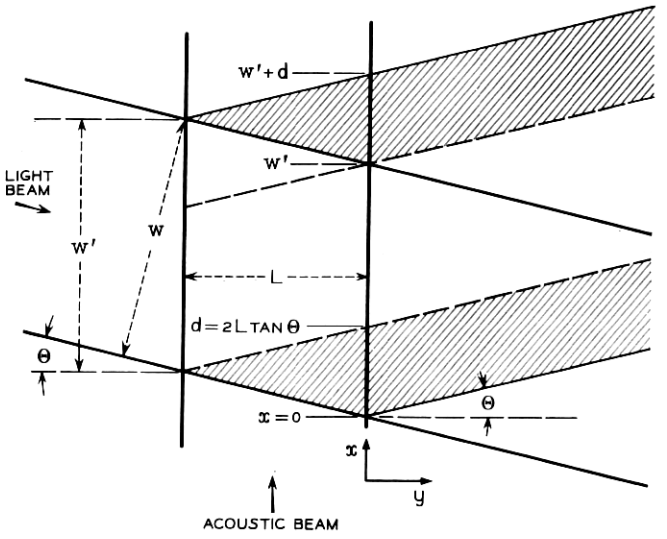

Fig. 13 — Uniform beam of finite width w incident at the Bragg angle.

Another distribution of interest because of experimental simplicity is the uniform beam of width w. With reference to Fig. 13, the near-field distribution of the scattered beam amplitude for interaction at the Bragg angle may be written as

$$\begin{aligned} E_1(\Theta,x) &= (x/d)\exp -\alpha x && 0 \leqq x < d \\ &= \exp -\alpha x && d \leqq x \leqq w' \\ &= [(w' + d - x)/d]\exp -\alpha x && w' < x \leqq w' + d \end{aligned} \tag{38}$$

in which $d = 2L \tan \Theta$ and $w' = w/\cos \Theta$. The far-field distribution can be written as

$$V_1(\eta) = \int_0^{w'+d} dx E_1(\Theta,x) \exp -i\alpha\eta x \tag{39}$$

which yields after some manipulation

$$V_1(\eta) = \left[\frac{1 - \exp -\alpha(1 + i\eta)w'}{\alpha(1 + i\eta)}\right]\left[\frac{1 - \exp -\alpha(1 + i\eta)d}{\alpha(1 + i\eta)d}\right]. \tag{40}$$

When the coherence width is sufficiently large that $\alpha d = 2\alpha L \tan \Theta \ll 1$, the scattered energy distribution has the form

$$| V_1(\eta) |^2 = \frac{1 + \exp -2\alpha w' - 2[\exp -\alpha w'] \cos \alpha w' \eta}{\alpha^2(1 + \eta^2)} . \quad (41)$$

Note that the angular distribution is Lorentzian only in the limit $\alpha w' \gg 1$. When $\alpha w'$ is not large, diffraction associated with the beam of width w modifies the line shape. (Even when $\alpha = 0$, if d/w' is not very small, the "edge effect" will change the far-field diffraction pattern.)

When αd is large so that the coherence width dominates, the line shape becomes a Lorentzian squared. In the intermediate region where αd is small but not negligible, one can write (40) in the form

$$| V_1(\eta) |^2 \approx \frac{1 - \alpha d + (1/12)\alpha^2 d^2[7 - \eta^2]}{1 + \eta^2} . \quad (42)$$

Thus the line shape is essentially Lorentzian except that the wings have a value somewhat less than that of a true Lorentzian.

2.3 *Experiment*

The experiments with finite α were performed using water at about 250 mc/s. The water cell consisted of two parallel quartz flats which were antireflection coated on the air side. Reflection at the quartz-water interface was negligible. One end of the water cell consisted of the fused quartz delay line described in Section I, which acted as a resonant buffer rod with evaporated-layer CdS as the longitudinal wave transducer. The opposite end of the cell was sufficiently far away that no reflections occurred. The traveling acoustic wave was square-wave modulated at 1 kc/s to allow synchronous detection of the scattered light.

A narrow slit was mounted in front of a photomultiplier and the entire assembly mounted on a micrometer-driven stage. The intensity distribution of the scattered light as well as that of the main beam could be mechanically scanned in the near or far field.

Near-field traces were taken with the slit as close to the water cell as possible; far-field traces were taken with the slit in the focal plane of a $\frac{1}{2}m$ focal length lens. The output of the phase-sensitive detector was applied to the Y axis of an X-Y recorder. The X axis was driven by the reference voltage from a Hewlett-Packard sweep drive unit attached to the micrometer stage. Visual confirmation of the recorder traces was made by observing the scattered light with a telescope focused on the cell for near field, and to infinity for the far field. The acoustically

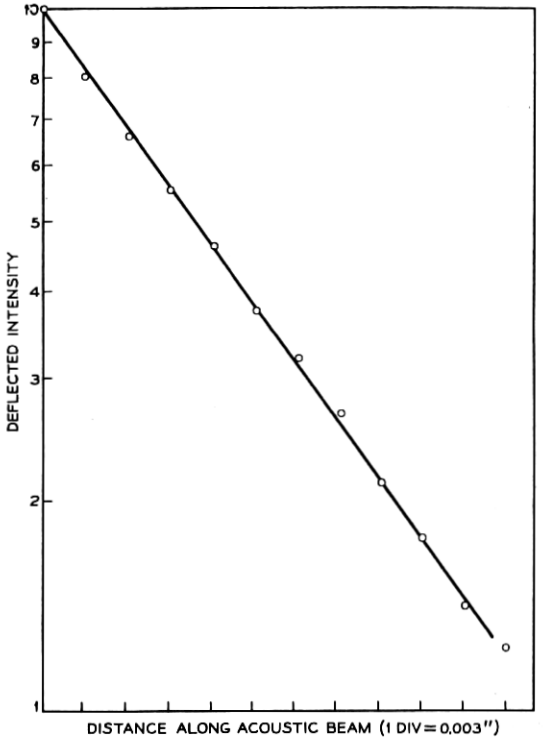

Fig. 14 — Deflected light intensity in arbitrary units vs distance along the acoustic beam.

scattered light could easily be distinguished from other "dirt" scattered light, since there was no granularity as is common for stationary scatterers.[5] Acoustic streaming[6] could also be observed.

As expected, the far-field diffraction of the acoustic beam, observed as described in Section I, exhibited little "coherence-width" degradation, i.e., the angular smear introduced by the term $\alpha \tan \theta_0$ in (26) was only 10^{-2} of the zero spacing. In what follows all observations were made at $\theta_0 = \Theta$.

The decay constant α was measured using a Gaussian beam from the laser and translating it along the acoustic beam. Fig. 14 is a semilog plot of the deflected intensity in arbitrary units vs distance. The curve yields the value $\alpha = 12.6$ cm^{-1}. For comparison, it is necessary to extrapolate values of α measured at lower frequency.[6] The measured value $\alpha/f^2 = 2.1 \times 10^{-16}$ (cm^{-1} sec^2) (f is the acoustic frequency = 245 mc/s) gives results in good agreement with the low-frequency results.

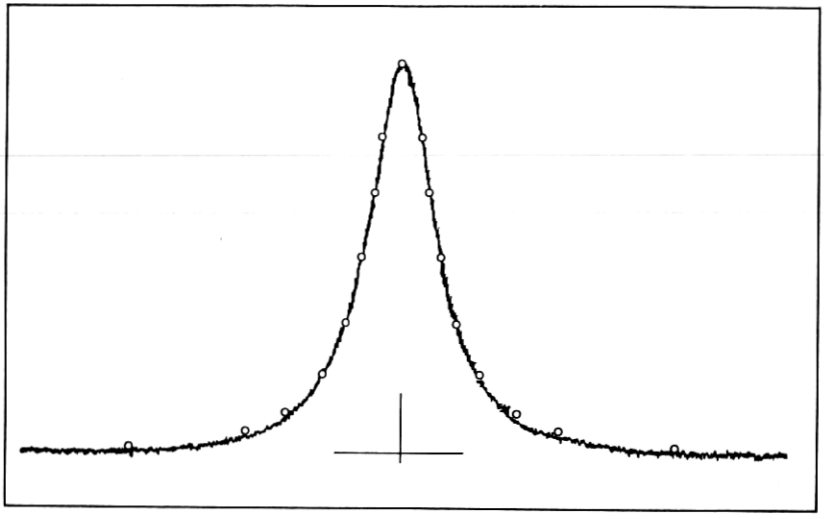

Fig. 15 — Far-field diffraction pattern of the beam scattered from a 245 mc/sec acoustic wave in water. The open circles correspond to a true Lorentzian matched to the peak and half-power points of the experimental curve.

The spot size of the Gaussian light beam was several times wider than the acoustic decay distance.

Near-field traces of scattered Gaussian, half-Gaussian, and uniform beams were obtained and gave results in qualitative agreement with the results of the previous section. No quantitative measurements were made.

Quantitative measurements were performed on the far-field pattern. A typical result is illustrated in Fig. 15 and was obtained with a half-Gaussian beam with a spot size in excess of one centimeter. The open circles are for a true Lorentzian matched to the experimental curve at the peak and half-power points. Note that the wings of the experimental curve are slightly less than the true Lorentzian value, as might be expected from the edge effect. The measured angular width [using (36)] agrees with the measured value of α within 5 per cent.

2.4 *Conclusion*

A technique for probing acoustic beams in optically transparent materials has been described. The technique is based on a Fourier transform relationship between the intensity distribution in the cross section of the acoustic beam and the angular dependence of the optical-acoustic interaction. It allows unequivocal determination of the volume

acoustic loss or phonon lifetime independent of the transducer and other boundary effects, precise determination of the average direction of the acoustic beam, and observation of the far-field diffraction pattern of the acoustic beam. It also determines the angular response of the transducer. When there is reason to believe that there is no phase shift in the cross-section, or if there is knowledge concerning the phase shift, the spatial distribution can be determined from the inverse Fourier transform of the measured angular distribution. Experiments illustrating and verifying these relationships have been described. Some of the far-field results for the scattered light intensity have relevance to optical beam deflection devices.[7]

ACKNOWLEDGMENT

The authors are greatly indebted to N. F. Foster, who fabricated the transducers used in these experiments.

APPENDIX

The amplitude of the incident Gaussian beam is given by

$$E_0(x,y) = \exp -\tfrac{1}{2}r^2/w^2.$$

Fig. 12 shows that for a beam incident at angle Θ with respect to the y axis

$$r = y \sin \Theta + x \cos \Theta$$

so that

$$E_0\,(x,y) = \exp -\tfrac{1}{2}\,\frac{(y \sin \Theta + x \cos \Theta)^2}{w^2}.$$

The scattered wave originating from $(x_0\,, 0)$ travels along the line $x = x_0 + y \tan \Theta$. The acoustic wave amplitude is given by $\exp -\alpha x$. The total scattered amplitude associated with the point $(x_0, 0)$ on the incident light beam can be written

$$E_1(\Theta,x_0) \propto \int_0^L dy \exp -\alpha(x_0 + y \tan \Theta) - \tfrac{1}{2}\,\frac{[y \sin \Theta + (x_0 + y \tan \Theta) \cos \Theta]^2}{w^2} \tag{42}$$

following the discussion in Section II. Multiplying out and completing the square in the exponential yields

$$E_1(\Theta,x_0) \propto \exp -\alpha x_0 - \tfrac{1}{2}\frac{x_0^2}{w^2}\cos^2\Theta + \frac{w^2}{8\sin^2\Theta}\left(\alpha\tan\Theta + \frac{x\sin 2\Theta}{w^2}\right)^2 \times \int_0^L dy \exp -\frac{2\sin^2\Theta}{w^2} \cdot\left[y + \left(\alpha\tan\Theta + \frac{x_0\sin 2\Theta}{w^2}\right)\frac{w_0^2}{4\sin^2\Theta}\right]^2. \tag{43}$$

With the substitution

$$y' = \left(y + \tfrac{1}{4}\left[\frac{\alpha w}{\cos\Theta} + \frac{2x_0}{w}\cos\Theta\right]\frac{w}{\sin\Theta}\right)\frac{\sqrt{2}\sin\Theta}{w}$$

(43) becomes

$$E_1(\Theta,x_0) \propto \exp -\alpha x_0 - \tfrac{1}{2}\frac{x_0^2}{w^2}\cos^2\Theta + \tfrac{1}{8}\left(\frac{\alpha w}{\cos\Theta} + \frac{2x_0\cos\Theta}{w}\right)^2 \times \frac{w}{\sqrt{2}\sin\Theta}\int_{\frac{\sqrt{2}}{4}\left[\frac{\alpha w}{\cos\Theta}+\frac{2x_0\cos\Theta}{w}\right]}^{\left(L+\frac{1}{4}\left[\frac{\alpha w}{\cos\Theta}+\frac{2x_0\cos\Theta}{w}\right]\right)\frac{w}{\sin\Theta}\frac{\sqrt{2}\sin\Theta}{w}} \exp -y'^2\,dy'. \tag{44}$$

This reduces to (30) upon substitution of

$$X = \sqrt{2}\left(\frac{L}{w}\right)\sin\Theta$$

$$Y = \tfrac{1}{4}\sqrt{2}\left(\frac{\alpha w}{\cos\Theta} + 2\left(\frac{x_0}{w}\right)\cos\Theta\right).$$

REFERENCES

1. Born, M., and Wolf, E., *Principles of Optics*, Pergamon Press, New York, 1959. Ch. 12 contains extensive bibliography and description of the earlier work.
2. Mason, W. P., *Piezoelectric Crystals and Their Application to Ultrasonics*, D. Van Nostrand Co., Princeton, N.J., 1950.
3. Fitch, A. H., and Dean, R. E., A Focusing Ultrasonic Delay Line, 1964 Symposium on Sonics and Ultrasonics, Santa Monica, Calif.
4. Quate, C. F., Shaw, H. J., Tien, P. K., Wilkinson, C. D. W., and Winslow, D. K., Diffraction of Laser Light with Hypersound, M.L. Report No. 1172, Microwave Laboratory, Stanford University, June, 1964.
5. Rigden, J. D., and Gordon, E. I., The Granularity of Scattered Optical Maser Light, Proc. IRE, *50*, Nov., 1962, p. 2367.
6. Herzfeld, K. F., and Litovitz, T. A., *Absorption and Dispersion of Ultrasonic Waves*, Academic Press, New York, 1959.
7. Cohen, M. G., and Gordon, E. I., Electro-Optic [$KTa_xNb_{1-x}O_3$(KTN)] Gratings for Light Beam Modulation and Deflection, Appl. Phys. Lett., *5*, 1964, p. 181.